Photoabsorption on nuclei in the energy range 0.5−2.6 GeV

V. Muccifora,* N. Bianchi,† A. Deppman, E. De Sanctis, M. Mirazita, E. Polli, and P. Rossi

INFN–Laboratori Nazionali di Frascati, P.O. Box 13, I-00044 Frascati, Italy

R. Burgwinkel, J. Hannappel, F. Klein, D. Menze, W. J. Schwille, and F. Wehnes

Physikalisches Insitut der Universitat Bonn, Nussallee 12, D-53155 Bonn, Germany

(Received 26 October 1998; published 16 November 1999)

The energy and nuclear mass dependences of the total hadronic cross section in the energy range 0.5–2.6 GeV have been measured at Bonn using the SAPHIR tagged photon beam. The measurement, performed on C, Al, Cu, Sn, and Pb, provides the first photoabsorption data in the region 1.2–1.7 GeV. The results show a significant reduction of the photoabsorption strength on the bound nucleon compared to the free-nucleon case in the whole energy region. Above 1.2 GeV this reduction decreases with the average nuclear density. [S0556-2813(99)01512-5]

PACS number(s): 25.20.Dc, 12.40.Vv

I. INTRODUCTION

The modification of the hadron properties and of the elementary couplings in the nuclear medium is one of the topics in nuclear physics currently addressed in various experimental and theoretical investigations.

The properties of baryon resonances in nuclei have been studied in recent photoabsorption experiments at Frascati [1–3], Mainz [4,5], and Bonn [6]. These showed significant medium effects: while the Δ resonance is only slightly distorted, higher excited nucleon states N^*, in the second and third resonance regions, are washed out. Furthermore, for photon energy $k>0.6$ GeV the absolute value of the cross section per nucleon is reduced, with respect to the free-nucleon case.

The mechanism of this damping is not yet well understood. In the resonance region (0.6–1.2 GeV) Fermi motion and Pauli blocking alone are unable to reproduce the resonance disappearance; therefore strong effects in the excitation, propagation, and interaction of the baryon [7] and meson [8,9] resonances in the nuclear medium are advocated. At higher energies vector meson dominance (VMD) models predict sizable shadowing effects starting from about 2 GeV [10–12].

In this paper are reported the results of the photoabsorption measurements on C, Al, Cu, Sn, and Pb performed at Bonn between 0.5 and 2.6 GeV. The cross sections for C and Pb have been already published [6]. Here the cross sections for the other nuclei are given along with the evaluation of the reduction and the average nuclear density dependence of the photoabsorption strength in different energy regions.

In Sec. II the experimental setup and method are extensively described. The analysis procedure is reported in Sec. III. In Sec. IV the results of the measurement are presented: specifically the cross sections, the ratio between photo-

nuclear and photonucleon cross sections, and the average nuclear density dependence.

II. EXPERIMENTAL SETUP AND METHOD

The photoabsorption measurements were performed using the photohadronic method. This method consists in measuring the photoproduction yield of hadronic events with a large solid angle detector, rejecting the vastly preponderant electromagnetic events by a separation using a forward angle shower detector. The photohadronic method was successfully applied in all previous measurements of the total photoabsorption cross section above the Δ-resonance excitation energy.

The measurement was carried out at Bonn using the SAPHIR tagged photon beam [13] of the ELSA accelerator and an apparatus similar to the one previously used at Frascati for nuclear photoabsorption measurements up to 1.2 GeV [3]. A schematic layout of the photon beam line and of the detector is given in Fig. 1.

A. Tagged photon beam

The photon beam was produced by the bremsstrahlung of electrons extracted from the ELSA accelerator into the SAPHIR beam line. The energy of the scattered electrons was measured in the tagging system TOPAS II which also supplied the trigger for the events. The tagging system consisted of a bremsstrahlung radiator, a dipole magnet, and a tagger made by two multiwire proportional chambers (MWPCs) placed in front of scintillation counters.

As a radiator (R) a copper foil $0.006X_0$ thick (X_0 being the radiation length) has been used. The dipole magnet had a maximum deflecting power of 1.2 T m, corresponding to a maximum end point energy $E_0=3.3$ GeV. For this measurement, the higher-energy-resolution information from the MWPC of the tagger was not used and the photon energy was reconstructed from the timing hodoscope only. The latter consisted of 14 scintillator counters (T1–T14), each 4.5 cm thick and different in size, providing a photon energy resolution ranging from about 9% for the lowest energies to

————
*Corresponding author. Electronic address: valeria.muccifora@lnf.infn.it
†Corresponding author. Electronic address: nicola.bianchi@lnf.infn.it
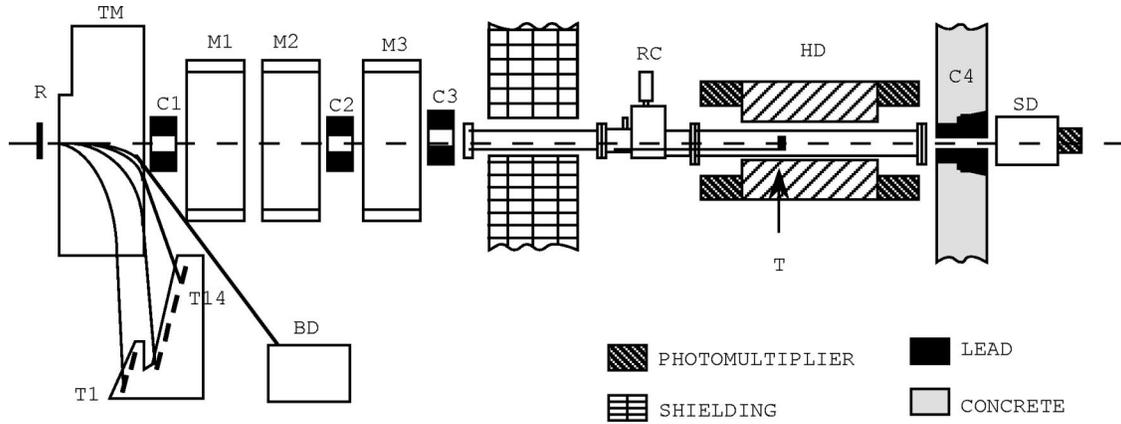
FIG. 1. Schematic layout side view of the experimental setup (not to scale). R, radiator; TM, tagging magnet; T1–T14, tagging counters; BD, beam dump; M1–M3, sweeping magnets; C1–C4, lead collimators; RC, remote control system for target movement; T, target; HD, hadron detector; SD, shower detector.

about 1% for the highest energies. The tagger covered the photon energy range $0.30E_0$–$0.95E_0$. In this experiment the photon energy range 0.5–2.6 GeV has been covered, with large overlapping regions at three electron beam energies E_0 = 1.6, 2.2, and 2.8 GeV.

The photon beam passed through a set of collimators and the SAPHIR apparatus. The three collimators C1–C3 defined a 1.5 cm diameter photon beam at the target position, while the three sweeping magnets M1–M3 strongly suppressed the charged background in the beam.

The lead glass shower detector SD allowed the simultaneous measurement of the tagged photon flux for each tagging channel. The photon beam intensity and the tagging efficiency (defined as the ratio between the number of tagged photons and the number of counts in the relevant tagging channel) were measured on line for each energy interval.

In Fig. 2 the tagging efficiencies of the 14 tagging channels measured at the three electron beam energies are shown. The values range between 0.73 and 0.92, depending on both the photon and electron beam energies. The decrease observed for the first channels (which correspond to the highest photon energies) is due to both Möller scattering and the background on the tagging counters. The decrease observed at the lowest electron beam energy is due to the wider bremsstrahlung photon emission angle and to the strong collimation cut.

The tagging efficiencies were found stable within $\approx 1\%$ during the whole data taking, as shown in Fig. 3 for two sample tagging channels.

B. Targets

Solid targets (T) of C, Al, Cu, Sn, and Pb were used. They had the form of disks 3 cm in diameter and thicknesses ranging between $0.08X_0$ for C to $0.2X_0$ for Pb (actual values are given in Table I).

The effective attenuation of the photon beam due to the electromagnetic interaction in the target was calculated for each nucleus as a function of the photon energy. The average photon beam attenuation ranged between 3% for C and 6.5% for Pb. The targets were individually mounted on a suitable

frame and moved into and off the photon beam by a remote control (RC) system.

In order to reduce effects due to possible changes in the electron beam, empty frame measurements were regularly interspersed inside a complete cycle of target runs and their contributions were subtracted. The empty frame yields, mainly ascribed to the photon beam interactions on materials along the beam line and on the target frame, were equivalent to less than 1 g cm^{-2} of lead and were found stable within $\approx 0.8\%$ during the whole measurement.

C. Detectors

A NaI crystal hadron detector (HD), consisting of four cylindrical sectors, each 60 cm long and 12 cm thick, surrounding the target, detected the charged hadrons and neutral mesons produced by the photon interaction in the target. The electromagnetically produced leptons and photons, mostly emitted close to the photon beam direction, were vetoed by the SD positioned about 1 m downstream to the target. Hadronic absorption of a photon of a given energy was indicated by a coincidence of signals from the relevant tagging channel and the HD without a simultaneous signal in the SD.
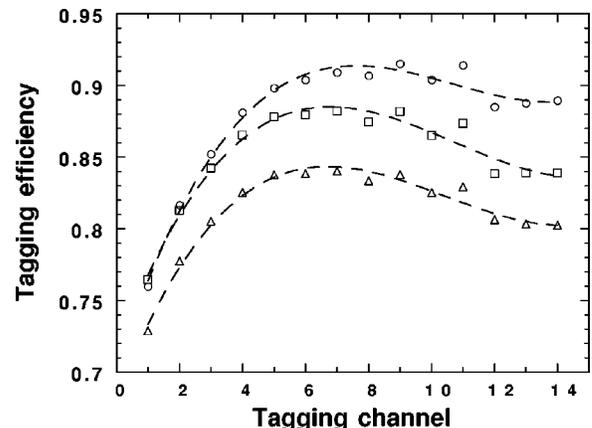
FIG. 2. Tagging efficiency of the 14 channels for the three different beam energies: 1.6 GeV (triangles), 2.2 GeV (squares), and 2.8 GeV (circles). Dashed curves are only guides for the eye.
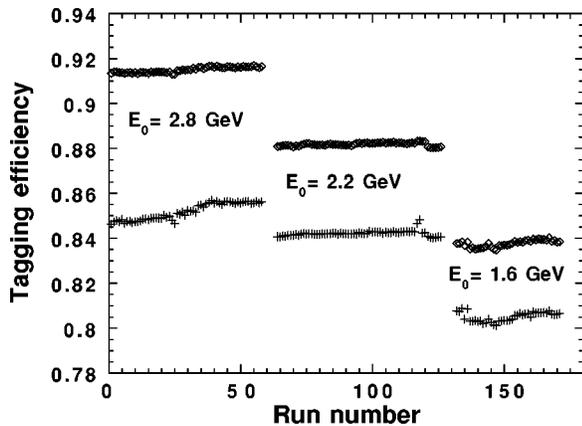
FIG. 3. Tagging efficiency of channels T3 (crosses) and T9 (diamonds) measured in each run for the three different beam energies.

The HD angular coverage was $8° < \theta < 169°$ for the polar angle and almost 2π for the azimuthal angle, which corresponds to more than 98% of the full solid angle. As a result of its thickness, the HD detected about 40% (30%) of the total energy carried by the hadrons produced by 0.5 GeV (2 GeV) photons. This energy is remarkably higher than that released in the HD by the products from electromagnetic events.

The SD consisted of a dense SF6 lead glass cylinder, 30 cm long and 12 cm in diameter. The large detector thickness ($19X_0$) provided an efficiency close to unity for detecting the electromagnetic showers generated from the photon beam and both the Compton photons and the lepton pairs produced off the target. The lead collimator C4, placed between the HD and the SD, defined a maximum polar angle of 2.4° with respect to the target center. This allowed us to detect both the beam photons and the electromagnetic products originating from the target, while strongly reducing the number of low-energy hadrons which might reach the SD. In addition, the threshold of the Čerenkov process in the SD provided a further rejection of low-energy hadrons.

D. Measurement

The photon energy range 0.5–2.6 GeV was covered with three different electron beam energies with widely overlap-

TABLE I. Target T, thickness [g/cm^2], yield (#) ($\times 10^4$), and average overall MC corrections (δ) at each electron beam energy E_0 [GeV]. The empty frame (EF) yield is also given.

T	Thickness	$E_0=1.6$		$E_0=2.2$		$E_0=2.8$	
		#	δ	#	δ	#	δ
C	3.450 ± 0.003	22	8.4%	60	5.8%	43	8.1%
Al	2.399 ± 0.004	20	8.0%	66	5.4%	43	7.2%
Cu	1.909 ± 0.013	19	7.6%	62	4.3%	50	6.2%
Sn	1.531 ± 0.011	25	5.8%	66	2.5%	53	5.0%
Pb	1.240 ± 0.016	35	2.7%	53	−0.4%	67	3.6%
EF		22		84		68	

ping photon energy regions. This allowed a check of the reproducibility of the measurements and gave an estimate of the systematic errors that could arise from different running conditions. Detector working parameters, such as HD and SD energy thresholds, were adjusted to optimize the efficiency of the hadron detection and to reduce the electromagnetic contamination at the different beam energies. The tagged photon beam rate was kept constant at 5×10^4 photons/s in order to reduce the random coincidence contamination. This amounted to about 1–6 % of the rate of true events, depending on both the target and the electron beam energy. Nevertheless, the random coincidences were on line measured and subtracted.

The number of events collected at the three electron energies, for the five targets and for the empty frame, are given in Table I.

III. PROCEDURE AND CORRECTIONS

The measured hadronic yields were very close to the absolute values of the total cross section, the off-line corrections being very small. The latter were due to (i) the loss of events with all hadrons emitted at a polar angle less than the minimum HD detection angle or depositing in the HD an energy below the threshold, (ii) HD contamination due to the products of unvetoed electromagnetic events with energy above the HD threshold, and (iii) SD contamination due to the events with hadrons releasing energy in both the HD and SD above the relevant thresholds.

In order to calculate the hadronic corrections (i) and (iii) a Monte Carlo (MC) simulation was developed, based on an intranuclear cascade model for photonuclear reactions. This code [14] accounts for the photon interaction with nucleons in the target through one-pion, two-pion, and multipion production processes in both resonant and nonresonant states; it simulates the intranuclear cascade of the photohadrons, which leaves the residual nucleus in an excited state that emits low-energy evaporation nucleons and light nuclei. The HD response function to the hadrons generated by this cascade-evaporative code was evaluated by using the GEANT-3.21 code. Figure 4 shows the simulated HD response function to the hadrons photoproduced on C and Al targets by 0.84–2.66 GeV photons. Also shown in the figure are the measured spectra with a threshold cut at 0.13 GeV. The simulated and measured spectra are in good agreement with each other. The broad peak shown at about 0.3 GeV is due to the hadronic events with at least one pion in the final state.

In order to evaluate the correction (ii), electromagnetic processes were simulated by using a modified version of the GEANT-3.21 code, where the experimental energy and angular distributions of pair production in the energy range of interest were explicitly introduced. In addition, Čerenkov photon emission, the attenuation of the Čerenkov light inside the lead glass, and the spectral response of the photomultipliers were taken into account.

Checks of the MC predictions were performed in order to test the effect of the energy and angular cuts on the efficiency and the acceptance of HD and SD.

The hadronic corrections, due to the finite angular accep-
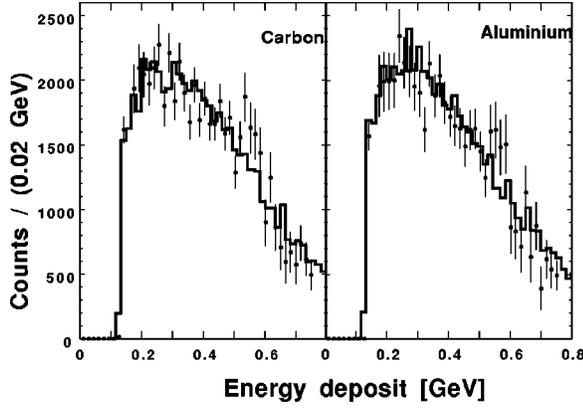
FIG. 4. Comparison between the simulated (histogram) and measured (solid circles) yield of the HD to 0.84–2.66 GeV photons on carbon and aluminum targets. The HD threshold setting was 0.13 GeV.

FIG. 6. The average C and Pb yields on all tagging channels, measured for different SD solid angle coverage. The notations are the same as for Fig. 5. The arrow indicates the solid angle relevant for the measurement.

tance of the HD and to the possible contamination of electromagnetic events not vetoed by the SD, were experimentally tested by varying the HD solid angle coverage. This was performed by moving the target upstream and downstream from the position used for the measurements. The comparison between the MC spectra and the experimental yields, for different HD solid angles, is shown in Fig. 5. The

FIG. 5. The average yield on all tagging channels (top) and on the three tagging channels at the lowest photon energies (bottom) measured for different HD solid angle coverage. The carbon data for $E_0 = 2.8$ GeV (open circles) and the lead data for $E_0 = 2.2$ GeV (solid circles) are compared with the MC predictions (dashed and solid lines, respectively). The arrow indicates the actual solid angle used for the measurement.

average yields for carbon and lead targets, measured at $E_0 = 2.8$ GeV and $E_0 = 2.2$ GeV, respectively, are given: the top panel refers to all tagging counters, while the bottom one to the three tagging channels at the lowest photon energies. In our geometry, the missing HD solid angle can be approximated as $\pi \theta_{min}^2$. The MC predictions have been parametrized in the form of $a - b \theta_{min}^2 + c / \theta_{min}^2$, where a is the total cross section, $-b \theta_{min}^2$ represents the loss of hadronic events in the forward HD hole, and $+c / \theta_{min}^2$ represents the electromagnetic contamination due to the $e^+ e^-$ pairs produced in the target. As shown in the figure, the hadronic losses are slowly increasing (yields decrease) as the missing HD solid angle increases, while the electromagnetic contamination becomes relevant only at a very small missing solid angle compared to the measurement position (yields increase). Moreover, this contribution is important only for the lead target and at the lowest photon energies. All the experimental yields are in good agreement with the MC predictions for both contributions.

The SD rejection efficiency as a function of the angular acceptance has been evaluated by measuring the yields for varied radii of the C4 collimator. These yields for carbon and lead, measured at $E_0 = 2.8$ GeV and $E_0 = 2.2$ GeV, respectively, are shown in Fig. 6 as a function of the forward solid angle $\Omega_{SD} \approx \pi \theta^2$ covered by the SD. The arrow indicates the actual solid angle used for the measurements. The MC predictions, parametrized in the form of $a + d / \Omega_{SD}$, agree quite well with the experimental points. As is shown, the hadronic cross section is constant in a broad range of solid angle values, thus indicating that electromagnetic events were adequately suppressed by the veto counter. An indication of the amount of the vetoed electromagnetic events is given by the yield value at $\Omega_{SD} = 0$ sr, measured by removing the SD veto.

Further experimental checks on the threshold efficiency of both the HD and SD detectors have been performed, finding a very good agreement with the MC predictions. These checks are extensively described in Ref. [15].

The results of the above-described checks validate the
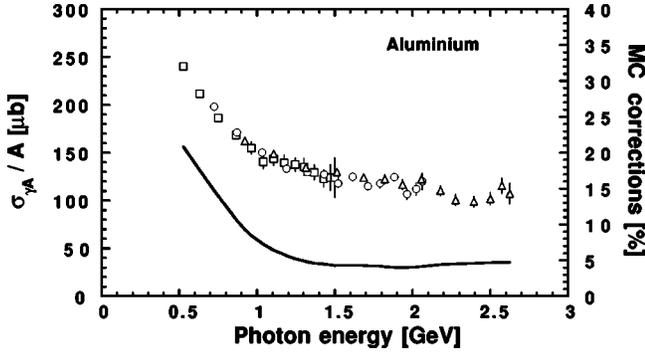
FIG. 7. Aluminum cross section measured at three electron beam energies: 1.6 GeV (squares), 2.2 GeV (circles), and 2.8 GeV (triangles), on the left scale, MC correction (solid line) due to the hadronic losses and electromagnetic contaminations on the right scale.

high reliability of the MC predictions. The average contributions of the whole corrections, as a percent of the yields for all the studied nuclei and at the three electron beam energies, are reported in Table I.

IV. RESULTS

A. Total cross sections

The cross section values were obtained by applying to the yields the previously described MC corrections. As an example of the quality of the data in Fig. 7 the cross section on aluminum, measured at the three electron beam energies, is shown together with the MC corrections: the latter remain almost constant at about 5% in the region of main interest for this measurement. As to be seen the three data sets are very consistent with each other.

The average values of the cross section in the overlapping regions are given in Table II for each nucleus. These values agree well with each other within the experimental errors for all the studied nuclei, showing the good control of the systematic errors. These mainly originate from the uncertainties in the target thickness (reported in Table I), the photon beam flux ($\approx 1\%$), the background subtraction ($\approx 1\%$ for C and $\approx 3\%$ for Pb), and the MC corrections ($\approx 1.5\%$ for C and $\approx 2.5\%$ for Pb). The total average systematic errors are

TABLE II. Average cross section $[\mu b/A]$ in the overlapping photon energy regions Δk [MeV] for the three beam energies E_0 [GeV] and for each target T. The errors are the quadratic sum of statistical and systematic uncertainties.

	$\Delta k=690-1480$		$\Delta k=830-1990$		$\Delta k=830-1480$	
T	E_0 1.6	E_0 2.2	E_0 2.2	E_0 2.8	E_0 1.6	E_0 2.8
C	156 ± 6	159 ± 4	137 ± 4	142 ± 4	151 ± 7	157 ± 8
Al	158 ± 8	159 ± 4	138 ± 5	142 ± 4	150 ± 8	153 ± 4
Cu	165 ± 10	163 ± 5	143 ± 6	147 ± 5	158 ± 11	157 ± 5
Sn	167 ± 11	164 ± 6	142 ± 6	144 ± 6	160 ± 11	155 ± 6
Pb	154 ± 12	153 ± 8	137 ± 8	144 ± 8	149 ± 13	147 ± 7

TABLE III. Total cross sections $[\mu b]$ and statistical errors normalized to the mass number A at the photon energy k [GeV]. The average value $\bar{A}$ is calculated weighting each nucleus cross section value with its statistical error.

	Total cross section /A					
k	C	Al	Cu	Sn	Pb	$\bar{A}$
0.53	229 ± 3	240 ± 3	244 ± 4	256 ± 4	271 ± 4	243 ± 2
0.63	197 ± 3	211 ± 3	208 ± 4	215 ± 4	213 ± 5	207 ± 2
0.73	192 ± 1	195 ± 2	195 ± 3	199 ± 2	180 ± 3	193 ± 1
0.87	170 ± 1	170 ± 2	176 ± 2	174 ± 3	160 ± 3	171 ± 1
0.93	169 ± 2	161 ± 3	169 ± 2	171 ± 3	154 ± 3	167 ± 1
1.07	150 ± 1	148 ± 2	153 ± 2	152 ± 2	142 ± 2	150 ± 1
1.19	139 ± 2	134 ± 3	142 ± 3	145 ± 3	134 ± 3	139 ± 1
1.32	134 ± 1	132 ± 2	136 ± 2	136 ± 3	133 ± 3	134 ± 1
1.43	126 ± 2	126 ± 3	134 ± 4	137 ± 5	133 ± 5	129 ± 2
1.54	123 ± 1	125 ± 2	134 ± 2	134 ± 3	132 ± 3	127 ± 1
1.70	121 ± 2	120 ± 3	126 ± 3	118 ± 4	130 ± 4	122 ± 1
1.83	112 ± 2	121 ± 3	122 ± 3	119 ± 4	122 ± 4	117 ± 1
1.96	114 ± 2	112 ± 3	118 ± 4	116 ± 4	119 ± 5	115 ± 1
2.06	114 ± 3	121 ± 5	112 ± 5	116 ± 6	110 ± 6	115 ± 2
2.18	116 ± 4	110 ± 5	114 ± 5	122 ± 6	119 ± 7	116 ± 2
2.28	114 ± 4	100 ± 6	115 ± 6	108 ± 7	107 ± 8	110 ± 3
2.39	111 ± 4	98 ± 5	107 ± 6	101 ± 7	109 ± 8	106 ± 2
2.50	122 ± 5	102 ± 7	117 ± 7	112 ± 8	122 ± 9	116 ± 3
2.59	109 ± 5	112 ± 7	101 ± 7	118 ± 9	124 ± 10	111 ± 3

$\approx 2\%$ for C and $\approx 5\%$ for Pb.

The cross section data measured at the three beam energies have been partitioned and averaged in 19 bins of energy about 100 MeV wide. The resulting total cross section values, normalized to the mass number A, are given in Table III for all the studied nuclei together with the statistical errors.

In the last column the weighted average of cross sections for the five nuclei is also given. This can be considered as the cross section on an average nucleus with $Z/A=0.469$ and an average nuclear density $\rho_A=0.109$ nucleons/fm^3. The photoabsorption cross sections are also shown in Fig. 8, together with the data for the proton [16]. The bars indicate the statistical errors only; the bands in the bottom of the panels represent the systematic uncertainties. The present data are in very good agreement within the experimental errors with both the low- and high-energy data available in the literature. They confirm, with reduced statistical uncertainties, the absence of peaks in the region of the second and third resonances for the bound nucleon. The new and most striking result is the persistence of the absorption strength reduction above 1.2 GeV compared to the free-nucleon case for all the studied nuclei.

B. Photonuclear to photonucleon cross section ratio

In order to better evaluate this strength reduction, the ratio between the nuclear cross section $\sigma_{\gamma A}$ and that obtained for the free nucleons ($Z\sigma_{\gamma p}+N\sigma_{\gamma n}$), derived from proton [16] and deuteron data [3,17], has been calculated in each energy region. These ratios are shown in Fig. 9, together with the
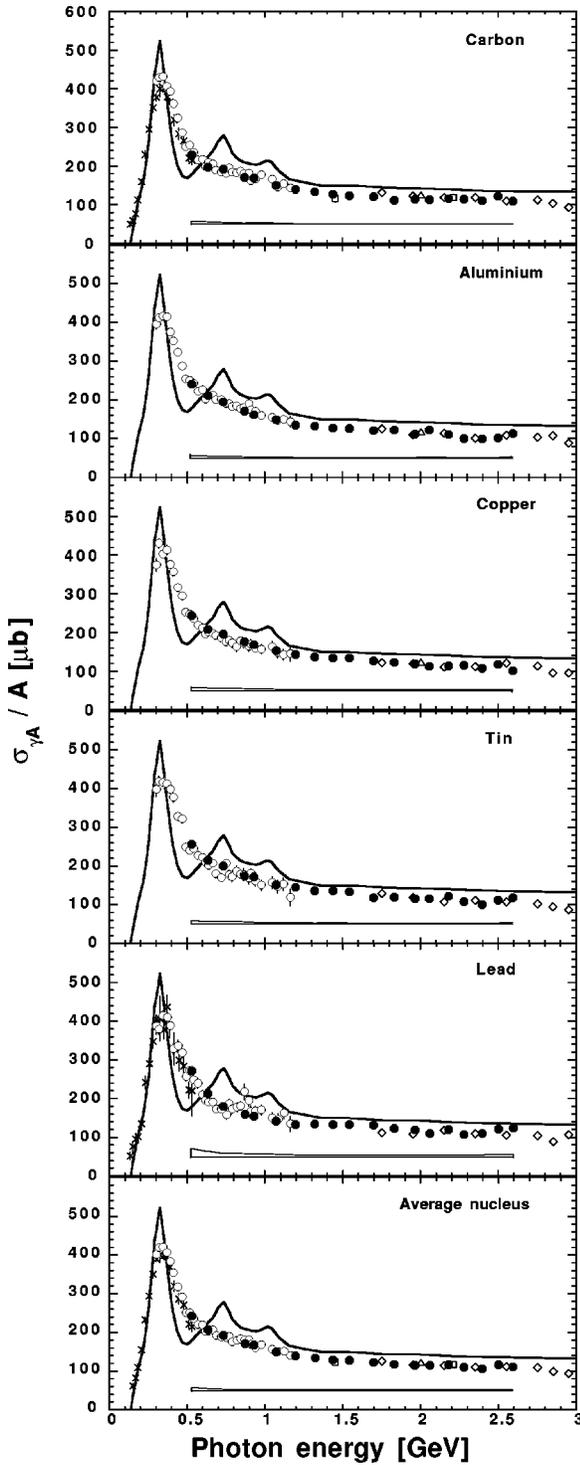
FIG. 8. Total cross section data on C, Al, Cu, Sn, and Pb, and average nucleus (solid circles) compared with data from previous experiments: crosses [18], open circles [3], squares [19], diamonds [20], and triangles [21]. Also shown is the proton absorption cross section [16] (solid line). The widths of the bands represent the systematic errors.

FIG. 9. Ratio of photonuclear and photonucleon absorption cross sections. Same notation as for Fig. 8. Solid line is a Δ-hole model [22]; dashed [11] and dotted [12] lines are VMD predictions. The bars represent the statistical errors.

results of a Δ-hole model [22] and of two recent VMD calculations for C, Cu, and Pb [11,12]. The former calculation reproduces well the experimental behavior at lower energies, while both VMD calculations do not predict the systematic

nuclear damping of the cross section clearly indicated by this experiment. In addition, the inclusion of two-nucleon correlations considered in Ref. [12] leads to an antishadowing behavior below 2 GeV and thus to an even larger disagreement with the data. In this respect, it has to be stressed that

TABLE IV. Energy regions, corresponding ranges and mean energies $\bar{k}$ [GeV], and average ratios $\bar{R}_A(\bar{k})$. The latter were computed by weighting $R_A(\bar{k})$ for each nucleus with its statistical error. In the last column, the statistical and systematic errors are also reported.

Energy region	Range	$\bar{k}$	$\bar{R}_A(\bar{k})$
Δ-resonance tail	0.48−0.68	0.58	$1.170 \pm 0.009 \pm 0.043$
D_{13} resonance	0.68−0.88	0.80	$0.771 \pm 0.004 \pm 0.021$
F_{15} resonance	0.88−1.25	1.00	$0.936 \pm 0.006 \pm 0.024$
Transition	1.25−1.65	1.40	$0.847 \pm 0.007 \pm 0.030$
Shadowing	1.65−2.65	2.00	$0.863 \pm 0.015 \pm 0.023$

the validity of the naive VMD model is doubtful at energies as low as 2 GeV.

C. Photoabsorption strength in the nuclear medium

For each nucleus the strength reduction was evaluated in the five energy regions given in Table IV. Both the integral $\Sigma_A(\bar{k})$ of the measured cross sections and the ratio $R_A(\bar{k}) = \Sigma_A/(Z\Sigma_p + N\Sigma_n)$ were calculated. Here $\bar{k}$ is the mean energy in each energy region and Σ_p and Σ_n are the proton and neutron cross sections integrated over the relevant photon energies.

In Table IV the averaged $\bar{R}_A(\bar{k})$, computed weighting $R_A(\bar{k})$ for each nucleus with its statistical error, is given. The energy behavior of $\bar{R}_A(\bar{k})$ is compared in Fig. 10(a) with the one derived from data from previous experiments. The comparison evidences the good agreement between data in both the resonance and the shadowing regions. In the transition between the resonance-excitation and the shadowing regions data from the present experiment evidence a photoabasorption strength reduction well above the experimental errors.

In addition, in each region the dependence of $\Sigma_A(\bar{k})$ on the average nuclear density ρ_A was parametrized in the form

$$\frac{\Sigma_A(\bar{k})}{A} = \Sigma_0(\bar{k})[1 + \beta(\bar{k})\rho_A]. \quad (1)$$

ρ_A was derived from the experimental charge density distributions using the rms electron-scattering radius $\overline{r^2}$ given in Ref. [24]. Different parametrizations of the nuclear density distribution result in an average variation of less than 5% in the ρ_A value.

In Fig. 10(b) the coefficients β obtained in each energy region from the fits to our data are shown together with the β we derived from the data from previous photoabsorption experiments. The energy behavior of β is similar to the one of $\bar{R}_A$ in the resonance region (below 1.25 GeV) and above 3 GeV. This indicates that the observed medium effect is proportional to the average nuclear density. On the contrary, in the transition region the β is positive while $\bar{R}_A$ is less than unity, indicating a stronger strength reduction in the light nuclei.
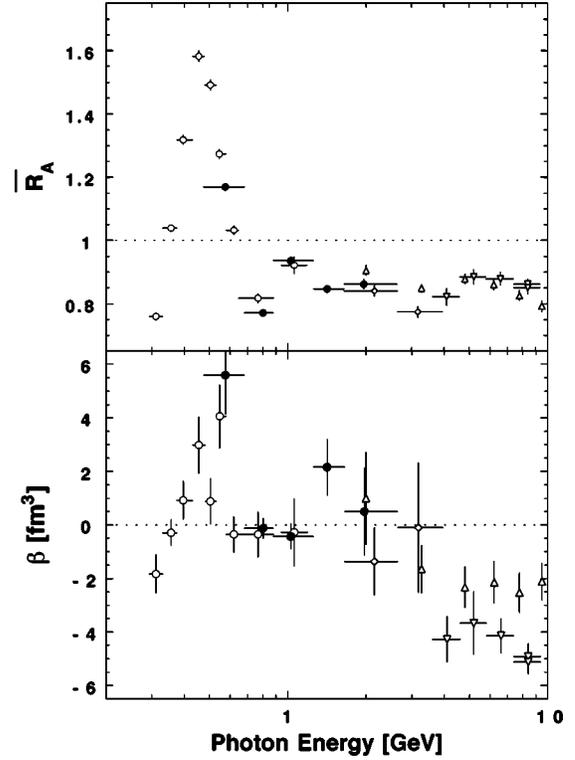
FIG. 10. (a) Average ratio $\bar{R}_A$ and (b) linear coefficient β derived from our data (solid circles), and from Refs. [3] (open circles), [20] (diamonds), [21] (upper triangles), and [23] (lower triangles). The vertical bars represent the statistical errors, while the horizontal bars represent the bin widths.

Similar information can be obtained also from different reactions, specifically from electron scattering at low four-momentum transfer $[Q^2 \leq 0.27 \; (\text{GeV}/c)^2]$ and from photon scattering at small angles. We have derived the β from measurements of these reactions performed on a wide range of mass number [25,26].

In Fig. 11 the β values are shown as a function of the real or virtual photon energy. The overall good agreement points
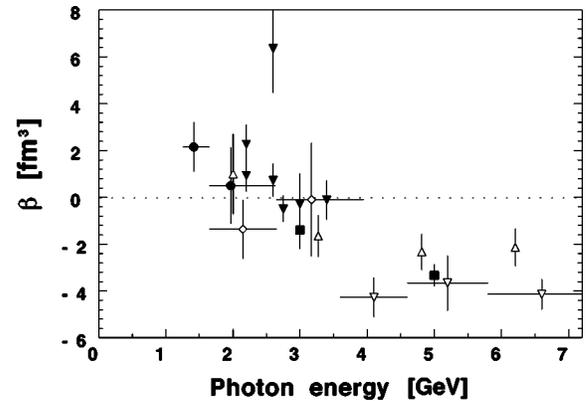
FIG. 11. Linear coefficient β derived from photoabsorption data (same notation as for Fig. 10), electron scattering [25] (solid triangles), and photon scattering [26] (solid squares) data. The vertical bars represent the statistical errors, while the horizontal bars represent the bin widths.

out the consistency of total photoabsorption, electron scattering, and photon scattering data.

In particular, below $\sim$2.6 GeV all the β, except the one derived from Ref. [20], are positive and this strengthens the evidence of a larger medium effect in light nuclei. This experimental finding may suggest in this region a mechanism for the strength reduction which does not depend on the average nuclear density alone.

V. CONCLUSIONS

The total photoabsorption cross section on C, Al, Cu, Sn, and Pb has been measured in the energy range 0.5–2.6 GeV.

The data confirm the absence of structures in the D_{13} and F_{15} resonance region and show the damping of the photoabsorption strength above 0.6 GeV compared to the free-nucleon case. The new result is the persistence of the strength reduction in the unexplored energy region 1.2–1.7 GeV, where resonance effects are expected to be small. In addition, our systematic measurement over a wide range of mass numbers indicates that in this region the strength reduction decreases with the average nuclear density.

[1] N. Bianchi *et al.*, Phys. Lett. B **309**, 5 (1993).

[2] N. Bianchi *et al.*, Phys. Lett. B **325**, 333 (1994).

[3] N. Bianchi *et al.*, Phys. Rev. C **54**, 1688 (1996).

[4] M. MacCormick *et al.*, Phys. Rev. C **53**, 41 (1996).

[5] M. MacCormick *et al.*, Phys. Rev. C **55**, 1033 (1997).

[6] M. Mirazita *et al.*, Phys. Lett. B **407**, 225 (1997).

[7] V. Muccifora, Nucl. Phys. **A623**, 116c (1997), and references therein.

[8] R. Rapp, M. Urban, M. Buballa, and J. Wambach, Phys. Lett. B **417**, 1 (1998).

[9] W. Peters, M. Post, H. Lenske, S. Leupold, and U. Mosel, Nucl. Phys. **A632**, 109 (1998).

[10] T.H. Bauer, R.D. Spital, D.R. Yennie, and F.M. Pipkin, Rev. Mod. Phys. **50**, 260 (1978).

[11] G. Piller, W. Ratzka, and W. Weise, Z. Phys. A **352**, 427 (1995).

[12] S. Boffi, Ye. Golubeva, L.A. Kondratyuk, and M.I. Krivoruchenko, Nucl. Phys. **A606**, 421 (1996); S. Boffi, Ye. Golubeva, L.A. Kondratyuk, M.I. Krivoruchenko, and E. Perazzi, Phys. At. Nucl. **60**, 1193 (1997).

[13] W.J. Schwille *et al.*, Nucl. Instrum. Methods Phys. Res. A **344**, 470 (1994).

[14] A.S. Iljinov, I.A. Pshenichnov, N. Bianchi, E. De Sanctis, V. Muccifora, M. Mirazita, and P. Rossi, Nucl. Phys. **A616**, 575 (1997).

[15] M. Mirazita, Ph.D. thesis, Milan University, 1998, Frascati Internal Report No. LNF-98/006.

[16] Particle Data Group, R.M. Barnett *et al.*, Phys. Rev. D **54**, 1 (1996), p. 191.

[17] D. Babusci, G. Giordano, and G. Matone, Phys. Rev. C **57**, 291 (1998).

[18] P. Carlos, in *Proceedings of the International School of Intermediate Energy Nuclear Physics*, Verona, 1985, edited by R. Bergère, S. Costa, and C. Schaerf (World Scientific, Singapore, 1985), p. 1.

[19] V. Heynen, H. Meyer, B. Naroska, and D. Notz, Phys. Lett. **34B**, 651 (1971).

[20] G.R. Brookes *et al.*, Phys. Rev. D **8**, 2826 (1973).

[21] S. Michalowski *et al.*, Phys. Rev. Lett. **39**, 737 (1977).

[22] R.C. Carrasco and E. Oset, Nucl. Phys. **A536**, 445 (1992).

[23] D.O. Caldwell *et al.*, Phys. Rev. D **7**, 1362 (1973); D.O. Caldwell *et al.*, Phys. Rev. Lett. **23**, 1256 (1969).

[24] C.W. De Jager, H. De Vries, and C. De Vries, At. Data Nucl. Data Tables **14**, 479 (1974).

[25] J. Bailey, D.R. Botterill, H.E. Montgomery, P.R. Norton, A. Del Guerra, A. Giazotto, M.A. Giorgi, A. Stefanini, and G. Matone, Nucl. Phys. **B151**, 367 (1979).

[26] L. Criegee, G. Franke, A. Giese, Th. Kahal, G. Poelz, U. Timm, H. Werner, and W. Zimmermann, Nucl. Phys. **B121**, 38 (1977).